Morphology control in semicrystalline solid polymer electrolytes for lithium batteries

Journal:	*Molecular Systems Design & Engineering*
Manuscript ID	ME-PER-02-2019-000028.R1
Article Type:	Perspective
Date Submitted by the Author:	02-May-2019
Complete List of Authors:	Li, Xiaowei; Drexel University, Materials Science and Engineering Cheng, Shan; Drexel University, Materials Science and Engineering Zheng, Yongwei; Drexel University, Materials Science and Engineering Li, Christopher; Drexel University, Materials Science and Engineering

Morphology control in semicrystalline solid polymer electrolytes for lithium batteries

Xiaowei Li, Shan Cheng, Yongwei Zheng and Christopher Y. Li *

Department of Materials Science and Engineering, Drexel University, Philadelphia, PA 19104, USA

*Corresponding author, C.Y. Li (Email: chrisli@drexel.edu. Tel: 215-895-2083. Fax: 215-895-6760)

Design, System, Application statement

Designing semicrystalline solid polymer electrolytes for lithium batteries applications is often hindered by the intertwining structural and dynamic effects of the semicrystalline morphology on the ionic conductivity and mechanical properties of the polymers. We show that these two effects can be quantitatively separated in the carefully designed polymer single crystal electrolytes. We further demonstrate that controlling crystalline morphology could be a viable approach to designing desired solid polymer electrolytes for lithium battery applications.

Morphology control in semicrystalline solid polymer electrolytes for lithium batteries

Xiaowei Li, Shan Cheng, Yongwei Zheng and Christopher Y. Li *

Department of Materials Science and Engineering, Drexel University, Philadelphia, PA 19104, USA

*Corresponding author, C.Y. Li (Email: chrisli@drexel.edu. Tel: 215-895-2083. Fax: 215-895-6760)

Abstract: Solid polymer electrolytes (SPEs) are one of the most promising solutions to the safety issues of lithium batteries. Understanding the morphology and dynamic effects on the ion transport properties of SPEs would be essential for future SPE design. In this article, using Poly(ethylene oxide) (PEO) as the example, we focus on the morphology control in semicrystalline SPEs. We show that the effect of semicrystallinity can be quantitatively separated into volume, structure and dynamic effects. We further demonstrate that morphological control plays an important role in ion transport control in semicrystalline SPE systems.

Introduction

Lithium-ion batteries (LIBs) are the systems of choice for portable electronic devices and they dominate our consumer market today.[1-4] A typical LIB represents a family of secondary (rechargeable) devices where both electrodes are intercalation materials, and the electrolyte is a lithium salt dissolved in a mixture of organic solvents. The advantages of LIBs include high energy density, flexible and light weight design and long lifespan. However, if lithium metal is used as the anode instead of lithium intercalation materials to fabricate a lithium metal battery (LMB), even higher power density can be achieved which is particularly critical for applications such as electric vehicles. Moreover, Li-O_2 and Li-S batteries show much higher theoretical specific energy (3,505 and 2,567 wh kg^{-1} for non-aqueous Li-O_2 and Li-S, respectively, vs. ~ 387 Wh kg^{-1} for today's commercial LIB).[5-7] Interestingly, fabrication of LMBs could be retrieved as early as 1970s. The system was proven not viable because the formation of Li dendrites during charge-discharge processes could potentially lead to explosion hazards.[1, 2] In order to circumvent this problem, intercalation materials instead of lithium metal were used as the anode whereas this stable operation was achieved by sacrificing power density. using solid polymer electrolytes (**SPEs**) to fabricate Li-layered oxide, Li-O_2 or Li-S batteries is an alternative approach to solve the safety issue without sacrificing power density due to the relatively high shear modulus of polymers, which could inhibit lithium dendrite formation and avoid the associated explosion hazard .[1-4, 8, 9] Monroe and Newman predicted that a homogeneous solid electrolyte with a modulus of **6-7 GPa** would completely suppress the formation of lithium dendrites.[10] This number was confirmed experimentally by Stone *et al.*[11] Based on this model, there have been extensive study on simultaneously tuning tuning mechanical properties and ionic conductivity in SPEs. However, recent work showed that LMBs and Li/SPE/Li symmetric cells using crosslinked SPEs with

various chemical designs are capable of cycling for prolonged time with excellent lithium dendrite resistance even with moderate mechanical modulus, suggesting that SPEs could be a viable system for future LMBs.[12-16]

Extensive theoretical and simulation works have been devoted to understating how ions are transported in entangled polymer melts.[17-20] In polymer electrolytes, different from classical liquid electrolytes, polymer chains are entangled and unable tophysically migrate "long distance" with the dissoluted ions. However, significant chain segmental motion exists above the glass transition temperature, and this motion would enable a solvation-desolvation process along the chain. Early simulation work shows that intra chain lithium ion motion, cooperative motion lithium ion-Poly(ethylene oxide) (PEO) complex, and intersegmental hopping between adjacent chains all contribute to lithium ion transport in PEO-based SPEs. [17-20 21] When segmental motion of the chain allows substitution of the anion site for an additional neighboring ligand, the charged pairs are separated and move in opposite directions which effectively allows ion transport in the polymer matrix. Therefore, the salt hosting polymers should have a high dielectric constant, high electron-donor characteristics and flexible backbone.[22, 23] PEO is one of the most extensively studied polymers for SPE applications because it exhibits superior ability to form complexes with a variety of metal salts.[22, 24-27] The EO unit (CH_2CH_2O) has strong electron donating capability and a desired heteroatom spacing, which facilitate the salt dissociation . The high flexibility of the PEO chain, due to the single C-O and C-C bonds in the backbone, allows for reorganization of the chain for cation coordination. Other polymers, such as poly(propylene oxide) (PPO), polysiloxanes, poly(ethylene succinate) and poly(ethylene imine), have also shown a certain capacity for complex formation with alkali metal salts, but are far less studied than PEO-based polyethers.[22, 25] Recent simulation also showed that stronger cation-polymer interactions facilitates ion dissociation and

improves conductivity.[28] It was further demonstrated that the tradeoff of improved ion solvent and impeded polymer dynamics upon increasing ion concentration leads to the observation of an optimal ion conductivity at moderate ion concentration.[29]

Crystalline morphology directed ion transport: bulk systems

At room temperature, the ionic conductivity of high molecular weight linear PEO-based SPEs is ~ 10^{-7}-10^{-9} S cm^{-1} while the acceptable value for battery application is ~ 10^{-4} S cm^{-1}. A common property tradeoff in SPEs is that the ionic conductivity decreases with increasing SPE shear modulus.[1, 2, 30-32] This tradeoff is often attributed to PEO crystallization. PEO is a well-known semicrystalline polymer with its glass transition temperature well below zero degree Celsius (*ca.* -60°C) and relatively high dielectric constant. Pristine PEO typically have a melting temperature of *ca.* 65 °C and a room temperature crystallinity of *ca.* 85% (i.e. 85% of the materials are in crystalline state). When mixed with alkali salts, three phases are defined: a crystalline PEO phase, an amorphous PEO-lithium complex phase, and a stoichiometric crystalline PEO-lithium complex phase. [33-41] **Figure 1a** shows the schematic of the three phases. The number and types of phases in a PEO/salt blend system depend on the type of anions, salt concentration and thermal history, and can be determined using X-ray diffraction, NMR, thermal analysis or polarized light microscopy (PLM).[35] **Figure 1b** shows the reported phase diagrams of a few commonly studied PEO-lithium salt SPEs.[35, 42] At high concentrations, PEO forms stoichiometric crystalline compounds with Li^+ cations and it was shown that crystalline complexes such as $P(EO)_6$:$LiXF_6$ (X= P, As, Sb) are quite conductive.[43-45] The structure of 6:1 crystalline complex ($P(EO)_6$:$LiAsF_6$) was resolved using powder diffraction, asshown in **Figure 2a**.[43-46] The crystalline complex adopts a monoclinic unit cell with two PEO chains interlocking to form cylinders with Li^+ cations residing in a row inside

each of the cylinders. The anions are located between the cylinders and do not coordinate with Li^+. As the anion size increases from PF_6^- to AsF_6^- to SbF_6^-, the volume of the unit cell expands by pushing the cylinders apart along *b* and *c* axis and stretching the polymer chain along the *a* axis.

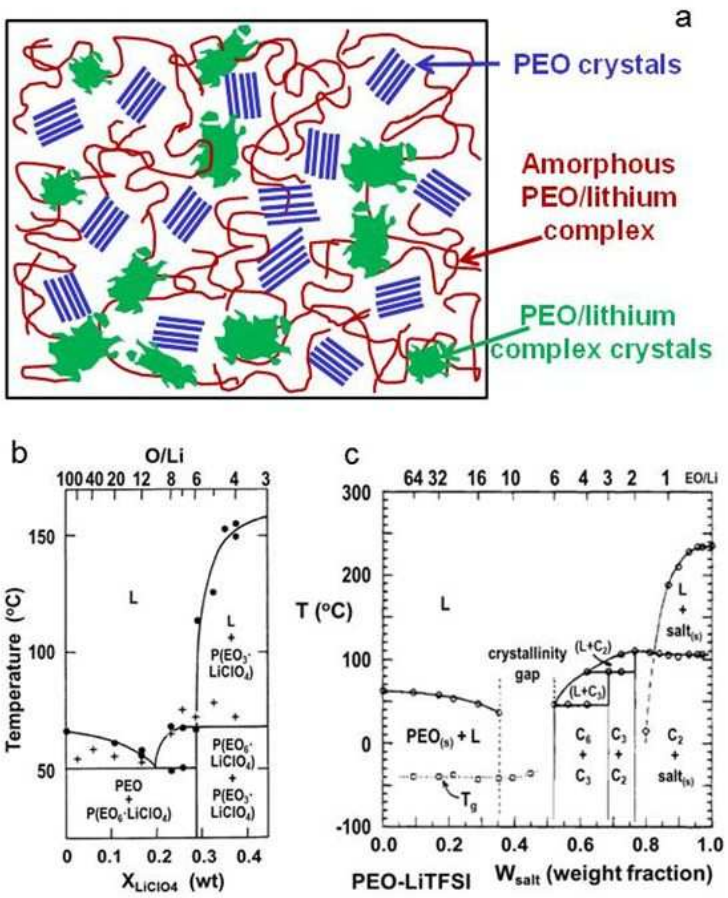

Figure 1. Phase structures in PEO/lithium salt electrolytes. (a) Three possible phases in semicrystalline PEO SPEs. (1) PEO crystals (blue), (2) amorphous PEO/salt complex (red), and (3) crystals of PEO/salt complex (green). (b-c) Phase diagrams of PEO-$LiClO_4$ and (c) PEO-LiTFSI. (b) is reprinted with permission from ***J. Electrochem. Soc.***, 133(2): 315-325 (1986). Copyright 1986, The Electrochemical Society; (c) is reprinted with permission from *Macromolecules*, 1994, 27, 7469-7477. Copyright (1994) American Chemical Society.

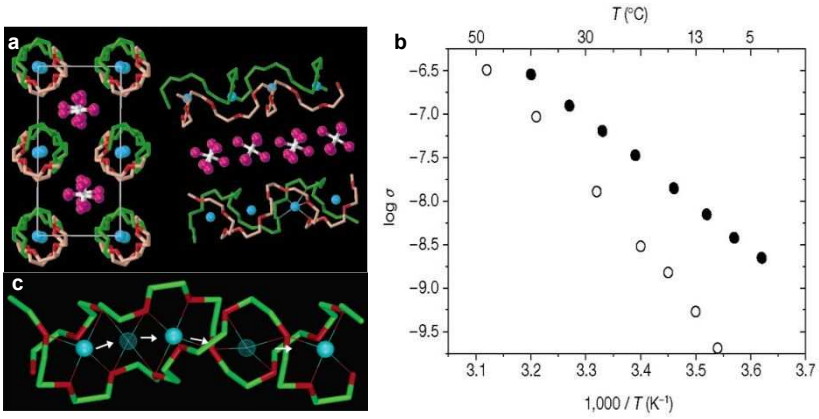

Figure 2. Structure and conductivity of PEO lithium salt complexes. (a) Crystal structure of $P(EO)_6$:$LiAsF_6$ crystalline complex; (b) Temperature dependent ionic conductivity of crystalline (solid circle) and amorphous (open circle) $P(EO)_6$:$LiSbF_6$; (c) Schematic illustration of Li^+ diffusion pathways in a $P(EO)_6$:$LiPF_6$ crystalline complex. (a) and (b) are reprinted by permission from Macmillan Publishers Ltd: *Nature*, 2001, 412, 520- 523, copyright (2001). (c) is reprinted with permission from *J. Am. Chem. Soc.*, 2003, 125, 4619-4626. Copyright (2003) American Chemical Society.

Figure 2b shows the temperature-dependent ionic conductivity of crystalline $P(EO)_6$:$LiSbF_6$, which shows a typical Arrhenius behavior, indicating that the ion hopping mechanism is dominating for the ion transport. The Li^+ diffusion pathway within the cylinder is shown in **Figure 2c** and the migration of Li^+ from one site to the neighboring site is facilitated by

the presence of vacancy defects. Despite that good ion conduction has been demonstrated in these crystalline complexes, the room temperature conductivities (10^{-7}~10^{-8} S cm^{-1}) are still low for lithium battery applications. Furthermore, to efficiently form these crystalline complexes with high conductivity, the PEO molecular weight used was *ca.* 1000 Da, relatively small for practical applications due to the poor mechanical properties of these oligomers. Further increasing the molecular weight significantly reduce ion conductivity because the increased population of grain boundaries and misalignment of the crystallites impede ion transport. Therefore, in the following discussion, we will focus on the PEO SPEs where these crystalline complex crystals are absent.

Based on the morphological understanding of the semicrystalline PEO SPEs, one "general rule" for designing high performance PEO-containing SPEs is to reduce polymer crystallinity by introducing short PEO groups whose melting point is lower than ambient temperature and they therefore are in the molten state at room temperature. Since these short PEO molecules are essentially liquid with poor mechanical properties, many studies have been conducted to improve the latter, including creating a short PEO-containing, crosslinked polymer network[47, 48] and using nanoparticles to reinforce PEMs.[49-53] Ceramic nanoparticles (e.g. TiO_2, SiO_2 or Al_2O_3) with Lewis acid characteristic can suppress the crystallization of polymer while their high modulus and high surface area can improve the mechanical properties. Another standout approach that has attracted extensive attention is block copolymer (BCP) SPEs.[1, 8, 54-67] BCPs consist of chemically different macromolecules (A & B) joined by covalent bonds at their ends to form a chain.[68-70] Due to the positive free energy of mixing A and B species, the respective blocks tend to segregate. The covalent linkage, however, prevents different segments from macrophase separation. Depending upon different volume ratios of each component, profound ordered structures can form as a result of this segregation process.[68-76] **Figure 3** shows the typical ordered structures of BCPs, including

sphere (S), cylinder (C), gyroid (G) and lamella (L) structures. From **Figure 3**, it is evident that if ions are in one phase while leaving the other phase mechanically robust, the mechanical and ion conducting properties are decoupled in BCP and materials with higher shear modulus and high ionic conductivity may be obtained. One can achieve this goal by synthesizing ion-containing BCPs [such as poly(styrenesulfonate) as the ion-containing block], or by blending lithium salts with PEO-containing BCPs. As previous discussed, while it was suggested that 6~7 GPa modulus of an SPE would sufficiently suppress lithium dendrite formation, the best battery device performance was achieved with a moderate SPE modulus of ~ a few tens of MPa. [12-16] It was also demonstrated that high toughness, high conductivity ion gels can be achieved by sequential triblock copolymer self assembly.[77] **Figure 3b** shows a micro phase separated structure of PEO-b-Polystyrene (PEO-*b*-PS). The PS block supports the electrolyte and the PEO phase forms a continuous network for lithium ion transport. During the past decade, extensive research efforts have been devoted to studying the structure-property relationship in BCP-based PEMs.[1, 8, 54-67] The conductivities in BCP SPEs are often estimated using the effective medium theory (EMT).[78] If one assumes that the ions are only located in one phase, the effective conductivity σ can be written as:

$$\sigma = f\phi_c\sigma_0 \qquad (1)$$

Where σ_0 and ϕ_c are the intrinsic conductivity and the volume fraction of the conducting phase, and *f* is the morphological factor. *f* is 2/3 and 1/3 for lamella and hexagonally packed cylinder structures, respectively. Note that this conclusion is based on the following assumptions: i) the length scale of the heterogeneities is much less than that of the medium; ii) the orientations of the small-scale domains are uncorrelated; and iii) the interaction at the domain interfaces is negligible. Numerous reports have shown that the morphological factor may be different from the values predicted by both theories, ranging from 0.01 – 0.67,[79, 80] and the discrepancies are typically

attributed to the poor connectivity between microdomains, which leads to lower measured conductivity for isotropic samples.[65, 79]

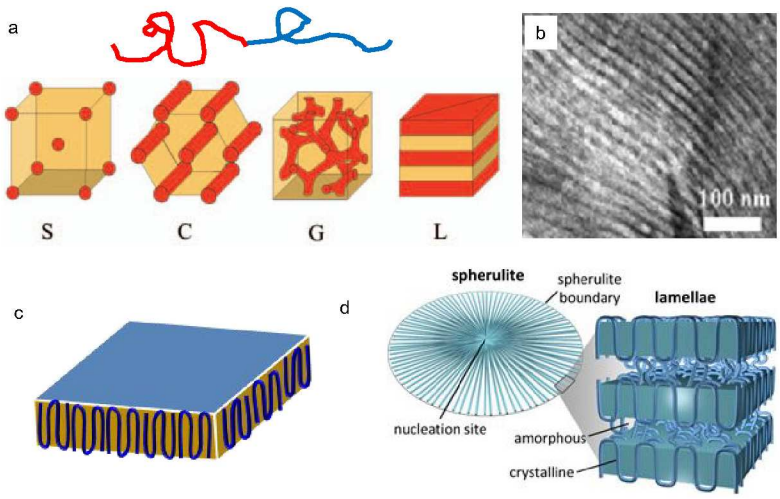

Figure 3. Comparing the morphologies of BCP SPEs and semicrystalline SPEs. (a) Phase structure of BCPs. (b) TEM images of a micro phase separated BCP SPE. (c-d) Schematics of a 2D polymer folded lamella and (d) polymer spherulites. The phase morphology and dimensions are analogous to lamellar BCPs. The TEM image is from *Macromolecules*, 2007, **40**, 4578-4585. Copyright (2007) American Chemical Society.

Morphology wise, semicrystalline SPEs are similar to the above discussed BCP SPEs – in semicrystalline polymers, chain folded lamellar crystals are the building blocks and they are quasi two-dimensional thin sheets with a typical thickness of *ca.* 10 nm and lateral dimension of *ca.* micrometers. These lamellae stack together and form spherulites which impinge at tens to hundreds of micrometers length scales. Amorphous chains are "confined" between adjacent

lamellae as shown in **Figures 3c,d**. On the molecular scale, this lamella/amorphous layer morphology is analogous to BCP lamellar structures – even the length scales are close. Furthermore, while pristine PEO has a degree of crystallinity as high as ~ 85%, it is significantly reduced, to a level of 10 - 30% after blending with lithium salts. PLM experiments reveal that PEO crystallizes into fringed spherulites in dilute SPE due to the strong interference with lithium salts.[21, 81-83] During the PEO crystallization process, lithium salts are expelled from the crystals and enrich the amorphous phase between adjacent spherulites, as well as in the amorphous inter-lamellar region. In semi-dilute electrolytes, both the PEO-lithium complex (salt-rich) and the PEO (salt-poor) phases crystallize into spherulitic morphology.[36, 38] This rather complex morphology affects ion transport properties of the SPE and the impact of crystallization are threefold: (i) decreasing the effective fraction of amorphous conducting phase; (ii) restricting chain mobility (dynamic/tethered chain effect) and (iii) imparting a tortuous pathway for ion transport (tortuosity effect). While the first aspect is directly related to crystallinity and relatively straightforward to understand, the second and third points are often intertwined.

Although extensive studies have been conducted to understand the correlation between crystallization and ionic conductivity reduction, obtaining quantitative analysis is challenging because those three factors, particularly the last two, are usually intertwined. The temperature dependent conductivity plots of semicrystalline PEO SPEs provide some useful information on the degree of conductivity reduction due to PEO crystallization. **Figure 4** shows the conductivity plots of a series of $P(EO)_n$:$LiClO_4$ electrolytes. A conductivity "knee" is observed for electrolytes at all concentrations around the PEO melting temperature, T_m (*ca.* 60 to 70 °C), below which the conductivity quickly drops to below 10^{-7} S cm^{-1}. This 2-3 orders of magnitude of conductivity reduction at room temperature results from the decrease of the conducting phase volume fraction,

restriction of chain mobility and the increased tortuosity as mentioned earlier, whereas the contributions from each factor cannot be quantitatively deconvoluted. All SPEs follow a typical Arrhenius behavior below the T_m of PEO, suggesting that the long-range polymer segmental motion is restricted and ion hopping is the major ion conducting mechanism. The steeper slopes at low temperatures indicate that there is a higher energy barrier for ion transport in semicrystalline SPEs.

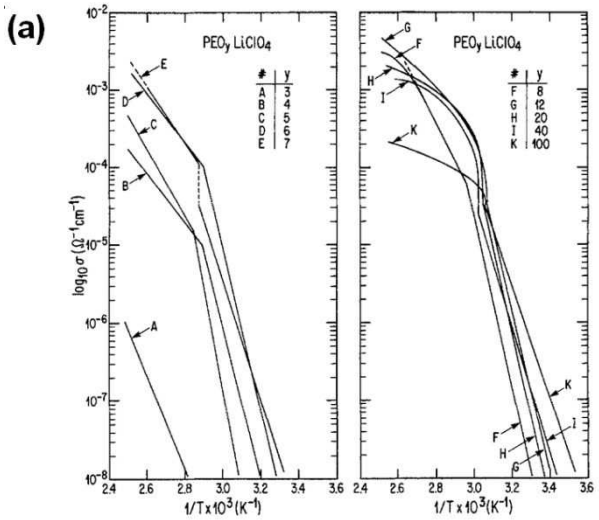

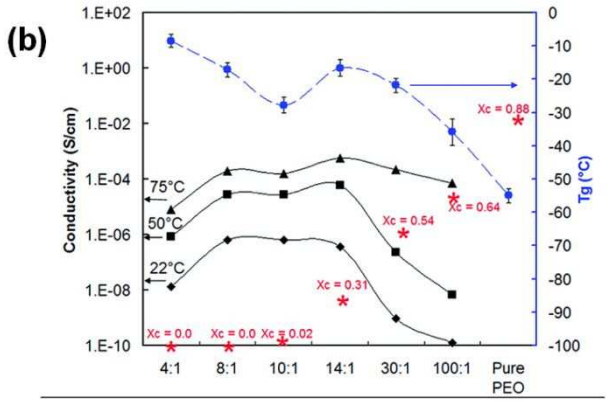

overall EO:Li	X_c (%)	T_g (°C)	effective EO:Li
8:1	0	−17	8:1
10:1	2	−28	10:1
14:1	31	−16.5	8:1

Figure 4. Temperature dependent ionic conductivity of PEO-lithium salts. (a) Temperature dependent ionic conductivity for solution cast P(EO)$_n$:LiClO$_4$ SPEs, reprinted with permission from *J. Electrochem. Soc.*, 133(2): 315-325 (1986). Copyright 1986, The Electrochemical Society. (b) Ionic conductivities, glass transition temperatures (T_g) and crystallinity (*) as a function of

$LiClO_4$ concentration at different temperatures for PEO-$LiClO_4$ SPE, adapted with permission from *Macromolecules*, 2009, 42, 2142-2156. Copyright (2009) American Chemical Society.

Although the highest ionic conductivity is expected to be in the completely amorphous state where the chain mobility is higher, Fullerton-Shirey *et al.* showed that the 14:1 (O/Li molar ratio) sample with 31% crystallinity has higher ionic conductivity than the 8:1 sample that is completely amorphous at 22 °C and 50 °C, respectively, though the effective Li^+ concentration (normalized by PEO crystallinity) and the T_g of the two SPE are the same.[84] Apparently in this case, the ion conduction is decoupled from chain mobility and the enhanced ionic conductivity in semicrystalline SPE indicates that there might be a faster ion transport in the amorphous conducting phase when confined by the PEO crystalline lamellae. The following section will discuss quantitative decoupling the dynamic and structure effect of semicrystalline morphology in SPEs.

Crystalline morphology directed ion transport: polymer single crystals

The most difficult issue to understand the crystallization effect on ion transport is the intertwining dynamic/tethered chain and tortuosity effect associated with the complex crystalline morphology. To quantitatively delineate these two effects, we recently designed a model polymer single crystal (PSC) SPE system.[85] As previously mentioned, PSCs are typically quasi 2D sheets. While originally used as a model system to study polymer crystal structure, they recently have been used for a variety of applications.[86-106] In our recent study, PEO single crystals were grown in dilute solution using a self-seeding method. Because of the well-controlled crystallization conditions, the obtained PSCs are *ca.* 20 × 20 μm wide (**Figure 5a**) and *ca.* 10 nm thick. A PSC

mat was obtained by solution casting the PSC suspension (**Figure 5b**). $LiClO_4$ was then infiltrated into the PEO single crystal films and the Li^+ concentration was $0.001 < r < 0.05$, where r is the molar ratio between Li^+ and EO group.

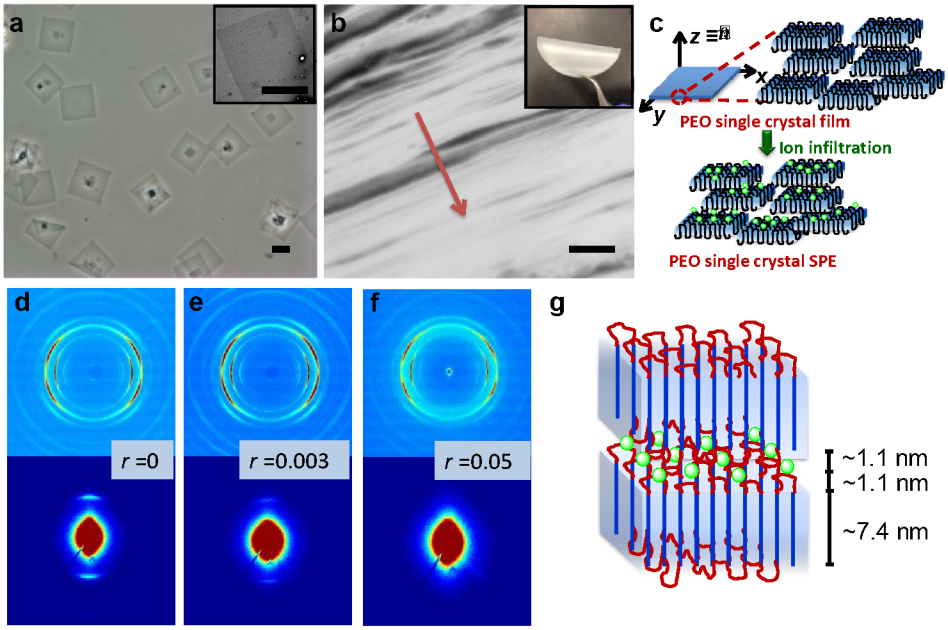

Figure 5. Design and fabrication of PSC SPE. (a) Phase contrast optical microscopy images of PEO single crystals; inset is a TEM image of one single crystal; scale bar is 10 μm. (b) Scanning electron microscopy image of the cross-section of PSC film; red arrow shows the film normal; scale bar is 200 nm. Inset shows a photo of the dry film. (c) Schematic of PSC SPE preparation. (d-f) 2D WAXD (top row) and SAXS (bottom row) patterns of selected PSC SPEs with Li to EO ratio r=0, 0.003 and 0.05, respectively. (g) Schematic illustration of the PSC SPE with the ions confined in the folded region.[85] Reprinted with permission from *Macromolecules*, 2014, 47, 3978-3986. Copyright (2014) American Chemical Society.

A 2-phase model with a PEO crystalline phase and an amorphous PEO/Li^+ salt phase was used to analyze the ion transport behavior: all the ions are confined in a 2D space with a thickness of ~ 2–3 nm (**Figure 5d-g**). In this case, since the crystalline domain does not complex with ions, a normalized *r* is defined as <*r*> (<*r*> ≡ *r/(1-X_c)*). Both in-plane conductivity $\sigma_{//}$ and through-plane conductivity $\sigma_{\perp}$ increase rapidly with <*r*> at low Li^+ ion concentrations (<*r*> < 0.02), and nearly plateau when <*r*> > 0.02 (**Figure 6**). The conductivity difference along these two directions can be quantified by defining an anisotropy factor as $A \equiv \sigma_{//}/\sigma_{\perp}$. At low <*r*> < 0.02, A is *ca.* 800-2000, indicating that the in-plane direction of the film is nearly three orders of magnitude more conductive than the through plane direction! The anisotropy gradually decreases to 100–300 when <*r*> is greater than 0.02. This interesting conductivity anisotropy was explained using a modified Nielsen's model, which is typically used to describe the relative permeability in polymer nanocomposites containing platelet–like nanofillers (**Figure 6a**):[107-109]

$$R_p = \frac{1-\phi_s}{1+\frac{L}{2W}\phi_s\left(\frac{2}{3}\right)\left(S+\frac{1}{2}\right)} = R_\sigma \qquad (2)$$

Here ϕ_s is the volume fraction of the filler which can be considered as the crystallinity in the present case, *L*/*W* is the aspect ratio of the filler, R_p is the relative permeability of the nanocomposite compared with pristine polymer, and *S* is order parameter of the filler. $A = \sigma_{//}/\sigma_{\perp} = R_{\sigma//}/R_{\sigma\perp}$ was calculated to be 668 at $\phi_s = 0.77$, and 521 at $\phi_s = 0.6$, which fits well with the measured anisotropy at the lower *r* region and is slightly higher than the measured value at the higher *r* region.

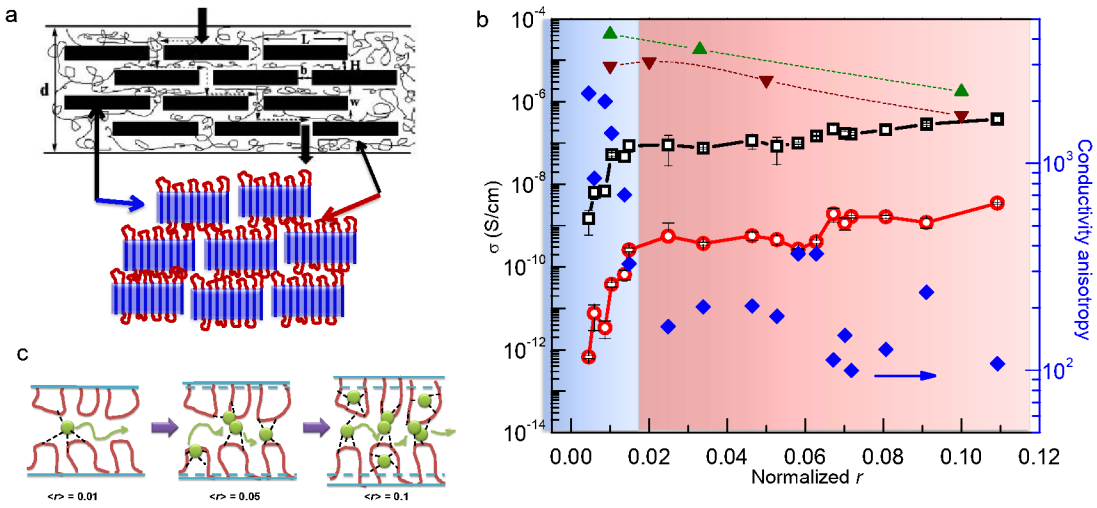

Figure 6. Anisotropic ion transport in PSC SPEs. (a) Comparison of the tortuous transport phenomenon in a polymer composite and PSC SPEs. (b) Room temperature ionic conductivity and conductivity anisotropy as a function of normalized *r*. (black open square – $\sigma_{//}$ of PSC SPE; red open circle – $\sigma_{\perp}$ of PSC SPE; blue solid diamond – A of single crystal SPE; green triangle – σ_0 of linear PEO-$LiClO_4$ SPE; brown inverted triangle – σ_0 of network PEO-$LiClO_4$ SPE from *ref*[110]) (c) shows that the cations are confined in the PEO fold regions at different concentration.[85] Reprinted with permission from *Macromolecules*, 2014, 47, 3978-3986. Copyright (2014) American Chemical Society.

The ability to measure the in-plane and through-plane conductivity of a well aligned polymer single crystal SPE film allows us to quantitatively delineate the structural and tortuosity effects of the crystalline morphology on ion transport. A generic expression for ionic conductivity of the semicrystalline SPE can be written as

$$\sigma = \frac{1}{k} \times \sigma_0 \times R_\sigma = \frac{1}{k} \times \sigma_0 \times \frac{1-\phi_s}{1+\frac{L}{2W}\phi_s\left(\frac{2}{3}\right)\left(S+\frac{1}{2}\right)} \quad (2)$$

where σ, σ_0 are the ionic conductivity for semicrystalline and the corresponding amorphous SPE. k factor was used to describe the dynamic effect and R_σ for the tortuosity factor, which accounts for the structural effect. While it is difficult to quantitatively evaluate the significance of each factor in a typical semicrystalline SPE bulk, in our model PSC SPEs, along the SPE film in-plane direction, structural/tortuosity effect is negligible and $\sigma_{//}$ can be simplified as:

$$\sigma_{//} \approx \frac{1}{k} \times \sigma_0 \times (1 - \phi_s) \qquad (3)$$

The dynamic effect can therefore be quantified by comparing σ_0 with $\sigma_{//}$ at a given <*r*>. k gradually decreases from *ca.* 180 at <*r*> = 0.0025 to *ca.* 1 at <*r*> = 0.05, suggesting that the conductivity reduction due to dynamic effect decreases from $10^1 \sim 10^2$ to near unity at moderate ion concentration, which is seemingly contradictory to the prevailing view that crystallization slows down the segmental dynamics of the polymer. This interesting observation can be explained by the unique structure of PSC folds. As shown in **Figure 6c**, in the PSC SPEs, the conducting phase only consists of rigid amorphous loops that attached on the lamellae surface, and ion conduction is achieved through hopping from one to another adjacent site. In the dilute ion region, the effective EO to Li ratio is *ca.* 100:1, and there are ~ 12 loops available for one Li^+ on the crystal surface and each Li^+ ion has to hop over ~ 2-3 loops to reach another ion as depicted in **Figure 6c**, which is energetically challenging. At higher salt concentrations, however, there is approximately one Li^+ ion per loop, allowing Li^+ to efficiently hop among PEO loops. The tethered chain effect is overwhelmed by the cross-linking introduced by the Li^+ ions themselves, and the only effect of crystallization on the overall conductivity of SPE is tortuosity. The design, characterization and interpretation of the anisotropic transport behavior of model PSC SPEs therefore quantitatively delineated the structure and dynamic effects of the semicrystalline morphology on ionic

conductivity. Note that in recent years, a series of polyethylene (PE) with precisely spaced with various functional groups have been reported and these polymers showed promising proton conductivity.[111, 112] For example, when sulfonic acid groups were introduced to every 21 carbons of the PE backbone (p21SA), its conductivity is similar to the gold standard Nafion 117, and it was proposed that the crystalline morphology of PE drives the formation of hairpin structure at the SA junctional, contributing to the high proton conductivity.[112] While this system dealt with proton instead of lithium transport, similar mechanisms could be applied to the lithium SPEs, and further confirms that chain folding and crystalline morphology could benefit ion transport.

Ion transport in semicrystalline hybrids/nanocomposite SPE

The incorporation of certain ceramic fillers such as TiO_2, SiO_2, or Al_2O_3 has been shown to enhance both ionic conductivity and mechanical properties of the SPEs.[49-53, 113-128] It has been reported that micro and nano sized ceramic particles can improve the mechanical properties, interfacial stability and ionic conductivity of SPEs, [49-53, 118, 121] while the conductivity enhancement due to the nanoparticles is not universal and contradictory results have been found in other SPEs.[129-131] For semicrystalline polymers, nanoparticles often significantly affect the polymer crystallization behavior, including structure, morphology, and crystallization kinetics.[132-135] Incorporating nanoparticles into the semicrystalline SPEs then also makes the quite complex transport system even more complicated, which to certain extends may contribute to the contradictory observations. Instead of going to the details of the complex morphology in semicrystalline SPEs, we will focus on the templating effect of 2D nanoparticles as this additional anisotropy of the filler allows us to better understand the ion transport in SPEs.

A few 2D fillers were introduced to SPEs in early studies. For example, montmorillonite and hectorite were compounded with polymer ion using solution infiltration, melt blending and layer–by–layer (LbL) assembly methods to fabricate hybrid SPEs.[136-139] 2D Graphene oxide (GO) nanosheets represent another interesting 2D filler and a few random oriented GO/PEO nanocomposite SPEs were reported with enhanced ion conductivity at relatively low GO concentrations.[140-143] In our recent work, anisotropic SPEs with GO fillers and GO-free $P(EO)_{12}$:$LiClO_4$ SPEs were prepared using a solution casting method where GO nanosheets were aligned parallel to the film surface upon solvent evaporation.[144] The PEO crystals in the GO-free SPEs exhibited moderate orientation, while the degree of PEO lamella orientation is considerably lower than that of the GO/PEO nanocomposite SPE. This morphological anisotropy directly led to the anisotropic conductivity as shown in **Figure 7.** In the high temperature region (T > 65 °C), all the polymer crystals are molten and there is no crystallization effect on the observed ionic conductivity, while in the low temperature region (near room temperature), crystallization plays a significant role.

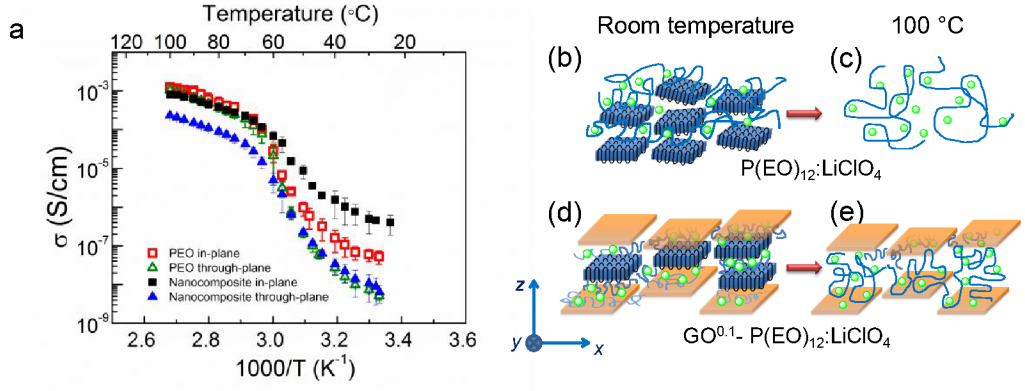

Figure 7. Anisotropic ion transport in 2D nanocomposite SPEs. (a) Temperature dependent ionic conductivity. Blue solid triangle ($P(EO)_{12}$:$LiClO_4$ in–plane), black open square ($GO^{0.1}$–$P(EO)_{12}$:$LiClO_4$ in–plane), red solid diamond ($P(EO)_{12}$:$LiClO_4$ through–plane), green open circle ($GO^{0.1}$–$P(EO)_{12}$:$LiClO_4$ through–plane). (b) Illustration of the crystalline structure change

of $P(EO)_{12}$:$LiClO_4$ (top) and $GO^{0.1}$-$P(EO)_{12}$:$LiClO_4$ (bottom) SPEs from room temperature (left) to 100 °C (right). Reprinted with permission from *Macromolecules*, 2015, **48**, 4503-4510. Copyright (2015) American Chemical Society.

Figure 7a allows us to approach the SPE ionic conductivity with (low temperature) and without (high temperature) the crystalline morphology effect. At high temperature, $\sigma_{//}$ and $\sigma_{\perp}$ curves of GO-free SPEs are overlapped, suggesting an isotropic transport while with GO, the SPEs show weak anisotropy of 4. The anisotropy of both SPEs increases as temperature decreases, *ca.* 10 and 70 for GO-free and nanocomposite SPEs, respectively. This suggests that the much greater anisotropy factor for the composite was due to GO-induced polymer crystallization. Both GO and PEO single crystals lie parallel to the film and collectively contribute to the conductivity anisotropy of 70 at room temperature. Since nanofiller induced polymer crystallization has been extensively studied, and the chain and polymer lamella orientation can be controlled by tuning the nanofiller orientation, this work therefore provides a feasible means to guide 2D lamellar orientation for ion transport control.

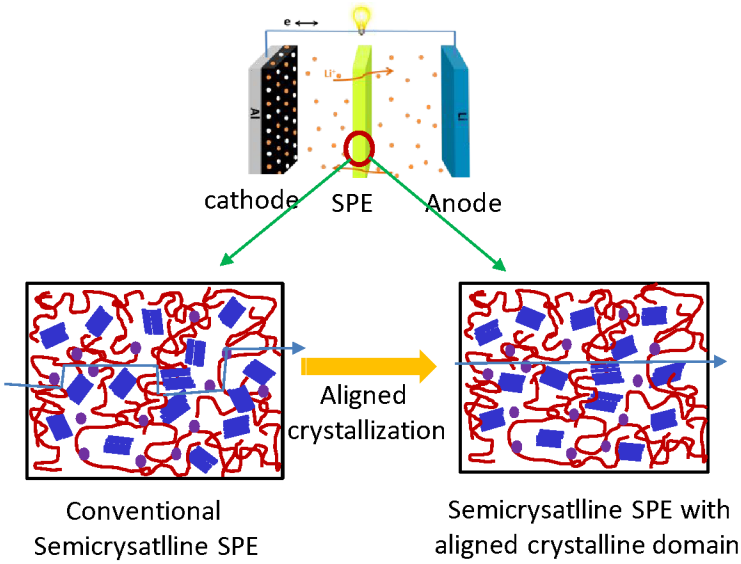

Figure 8. Schematics of suggested semicrystalline SPE design. Proper alignment of the crystalline domain can minimize the tortuosity effect of crystalline domain on ion transport, leading to SPEs with improved conductivity without sacrificing mechanical properties.

Summary and outlook

In this article, we briefly summarized the morphology effect on ion transport in semicrystalline SPEs. Nanoscale morphology is complex in semicrystalline SPEs and plays an essential role in their electrochemical performance. Recent work showed that crystalline lamellae in semicrystalline SPEs confine and direct ion transports. The in-plane conductivity is *ca.* three orders of magnitude greater than the through-plane ones. More interestingly, at a moderate ion concentration, the dynamic effect of the crystalline morphology is negligible, and the crosslinking effect of the ion dominates the system. This suggests that in order to design semicrystalline SPEs for practical applications, controlling the morphology is of utter importance (Figure 8). Since the crystalline portion of the materials provides the indispensable mechanical properties, semicrystalline SPEs have their own advantages in SPE design when comparing with other

systems such as BCP SPEs. It is also of interest to investigate anisotropic mechanical properties in semicrystalline SPEs with aligned crystalline domains. To further improve the overall properties of semicrystalline SPEs, one can borrow classical polymer processing methods, for example, introducing anisotropic nucleating agent to direct polymer crystallization. Mechanical field and temperature gradient could also potentially assist polymer crystallization.

Acknowledgements

We are grateful for the support from the National Science Foundation through grants CBET 1510092 and CBET 1603520.

Conflicts of interest

The authors declare no conflicts of interest.

References

1. J. M. Tarascon and M. Armand, *Nature*, 2001, **414**, 359-367.
2. M. Armand and J. M. Tarascon, *Nature*, 2008, **451**, 652-657.
3. E. Quartarone and P. Mustarelli, *Chem. Soc. Rev.*, 2011, **40**, 2525-2540.
4. J. B. Goodenough and Y. Kim, *Chem. Mater.*, 2010, **22**, 587-603.
5. P. G. Bruce, S. A. Freunberger, L. J. Hardwick and J.-M. Tarascon, *Nature Materials*, 2012, **11**, 19-29.
6. S. A. Freunberger, Y. Chen, N. E. Drewett, L. J. Hardwick, F. Barde and P. G. Bruce, *Angew. Chem. Int. Ed.*, 2011, **50**, 8609-8613.

7. M. M. O. Thotiyl, S. A. Freunberger, Z. Peng and P. G. Bruce, *J. Am. Chem. Soc.*, 2013, **135**, 494-500.
8. M. A. Hickner, *Mater. Today*, 2010, **13**, 34-41.
9. P. G. Bruce, B. Scrosati and J. M. Tarascon, *Angew. Chem. Int. Ed.*, 2008, **47**, 2930-2946.
10. C. Monroe and J. Newman, *J. Electrochem. Soc.*, 2005, **152**, A396-A404.
11. G. M. Stone, S. A. Mullin, A. A. Teran, D. T. Hallinan, A. M. Minor, A. Hexemer and N. P. Balsara, *J. Electrochem. Soc.*, 2012, **159**, A222-A227.
12. M. D. Tikekar, L. A. Archer and D. L. Koch, *J. Electrochem. Soc.*, 2014, **161**, A847-A855.
13. Q. Pan, D. M. Smith, H. Qi, S. Wang and C. Y. Li, *Adv. Mater.*, 2015, **27**, 5995-6001.
14. Q. Pan, D. Barbash, D. M. Smith, H. Qi, S. E. Gleeson and C. Y. Li, *Adv. Energy Mater.*, 2017, **7**, 1701231-n/a.
15. Y. Zheng, Q. Pan, M. Clites, B. W. Byles, E. Pomerantseva and C. Y. Li, *Adv. Energy Mater.*, 2018, **8**, 1801885.
16. M. D. Tikekar, S. Choudhury, Z. Tu and L. A. Archer, *Nature Energy*, 2016, **1**, 16114.
17. V. Ganesan, *Mol. Sys. Des. Engin.*, 2019.
18. S. Mogurampelly, O. Borodin and V. Ganesan, *Annu. Rev. Chem. Biomol. Engin.*, 2016, **7**, 349-371.
19. K.-J. Lin and J. K. Maranas, *Macromolecules*, 2012, **45**, 6230-6240.
20. K.-J. Lin and J. K. Maranas, *Phys. Rev. E*, 2013, **88**, 052602.
21. Z. Xue, D. He and X. Xie, *J. Mater. Chem. A*, 2015, **3**, 19218-19253.
22. M. B. Armand, *Annu. Rev. Mater. Sci.*, 1986, **16**, 245-261.
23. W. H. Meyer, *Adv. Mater.*, 1998, **10**, 439-448.
24. M. A. Ratner and D. F. Shriver, *Chem. Rev.*, 1988, **88**, 109-124.
25. M. Armand, *Solid State Ionics*, 1983, **9–10, Part 2**, 745-754.
26. D. Baril, C. Michot and M. Armand, *Solid State Ionics*, 1997, **94**, 35-47.
27. M. Armand, *Adv. Mater.*, 1990, **2**, 278-286.
28. B. K. Wheatle, N. A. Lynd and V. Ganesan, *ACS Macro. Lett.*, 2018, **7**, 1149-1154.
29. B. K. Wheatle, J. R. Keith, S. Mogurampelly, N. A. Lynd and V. Ganesan, *ACS Macro. Lett.*, 2017, **6**, 1362-1367.
30. M. Armand, *Solid State Ionics*, 1994, **69**, 309-319.
31. M. Armand, *Adv. Mater.*, 1990, **2**, 278-286.
32. M. Armand, *Sol. St. Ion.*, 1983, **9-10**, 745-754.
33. D. R. Payne and P. V. Wright, *Polymer*, 1982, **23**, 690-693.
34. C. Berthier, W. Gorecki, M. Minier, M. B. Armand, J. M. Chabagno and P. Rigaud, *Solid State Ionics*, 1983, **11**, 91-95.
35. C. D. Robitaille and D. Fauteux, *J. Electrochem. Soc.*, 1986, **133**, 315-325.
36. R. Neat, M. Glasse, R. Linford and A. Hooper, *Solid State Ionics*, 1986, **18–19, Part 2**, 1088-1092.
37. M. Marzantowicz, J. R. Dygas, F. Krok, A. Łasińska, Z. Florjańczyk, E. Zygadło-Monikowska and A. Affek, *Electrochim. Acta*, 2005, **50**, 3969-3977.
38. M. Marzantowicz, J. R. Dygas, F. Krok, J. L. Nowiński, A. Tomaszewska, Z. Florjańczyk and E. Zygadło-Monikowska, *J. Power Sources*, 2006, **159**, 420-430.
39. M. Marzantowicz, J. R. Dygas, F. Krok, Z. Florjańczyk and E. Zygadło-Monikowska, *Electrochim. Acta*, 2007, **53**, 1518-1526.
40. M. Marzantowicz, F. Krok, J. R. Dygas, Z. Florjańczyk and E. Zygadło-Monikowska, *Solid State Ionics*, 2008, **179**, 1670-1678.
41. G. Zardalidis, E. Ioannou, S. Pispas and G. Floudas, *Macromolecules*, 2013, **46**, 2705-2714.
42. S. Lascaud, M. Perrier, A. Vallee, S. Besner, J. Prud'homme and M. Armand, *Macromolecules*, 1994, **27**, 7469-7477.
43. G. S. MacGlashan, Y. G. Andreev and P. G. Bruce, *Nature*, 1999, **398**, 792-794.
44. Z. Gadjourova, Y. G. Andreev, D. P. Tunstall and P. G. Bruce, *Nature*, 2001, **412**, 520-523.

45. Z. Stoeva, I. Martin-Litas, E. Staunton, Y. G. Andreev and P. G. Bruce, *J. Am. Chem. Soc.*, 2003, **125**, 4619-4626.
46. Z. Gadjourova, D. Martín y Marero, K. H. Andersen, Y. G. Andreev and P. G. Bruce, *Chem. Mater.*, 2001, **13**, 1282-1285.
47. J. Cui, M. A. Lackey, G. N. Tew and A. J. Crosby, *Macromolecules*, 2012, **45**, 6104-6110.
48. C. N. Walker, C. Versek, M. Touminen and G. N. Tew, *ACS Macro. Lett.*, 2012, **1**, 737-741.
49. F. Capuano, F. Croce and B. Scrosati, *J. Electrochem. Soc.*, 1991, **138**, 1918-1922.
50. F. Croce, G. B. Appetecchi, L. Persi and B. Scrosati, *Nature*, 1998, **394**, 456-458.
51. F. Croce, R. Curini, A. Martinelli, L. Persi, F. Ronci, B. Scrosati and R. Caminiti, *J. Phys. Chem. B*, 1999, **103**, 10632-10638.
52. G. B. Appetecchi, F. Croce, L. Persi, F. Ronci and B. Scrosati, *Electrochim. Acta*, 2000, **45**, 1481-1490.
53. F. Croce, L. Persi, B. Scrosati, F. Serraino-Fiory, E. Plichta and M. A. Hendrickson, *Electrochim. Acta*, 2001, **46**, 2457-2461.
54. Y. A. Elabd and M. A. Hickner, *Macromolecules*, 2011, **44**, 1-11.
55. J. R. M. Giles, F. M. Gray, J. R. Maccallum and C. A. Vincent, *Polymer*, 1987, **28**, 1977-1981.
56. F. M. Gray, J. R. MacCallum, C. A. Vincent and J. R. M. Giles, *Macromolecules*, 1988, **21**, 392-397.
57. P. P. Soo, B. Y. Huang, Y. I. Jang, Y. M. Chiang, D. R. Sadoway and A. M. Mayes, *J. Electrochem. Soc.*, 1999, **146**, 32-37.
58. A. V. G. Ruzette, P. P. Soo, D. R. Sadoway and A. M. Mayes, *J. Electrochem. Soc.*, 2001, **148**, A537-A543.
59. P. E. Trapa, B. Y. Huang, Y. Y. Won, D. R. Sadoway and A. M. Mayes, *Electrochemical and Solid State Letters*, 2002, **5**, A85-A88.
60. P. E. Trapa, Y. Y. Won, S. C. Mui, E. A. Olivetti, B. Y. Huang, D. R. Sadoway, A. M. Mayes and S. Dallek, *J. Electrochem. Soc.*, 2005, **152**, A1-A5.
61. H. Kosonen, S. Valkama, J. Hartikainen, H. Eerikainen, M. Torkkeli, K. Jokela, R. Serimaa, F. Sundholm, G. ten Brinke and O. Ikkala, *Macromolecules*, 2002, **35**, 10149-10154.
62. T. H. Epps, T. S. Bailey, R. Waletzko and F. S. Bates, *Macromolecules*, 2003, **36**, 2873-2881.
63. T. Niitani, M. Shimada, K. Kawamura, K. Dokko, Y. H. Rho and K. Kanamura, *Electrochemical and Solid State Letters*, 2005, **8**, A385-A388.
64. M. Singh, O. Odusanya, G. M. Wilmes, H. B. Eitouni, E. D. Gomez, A. J. Patel, V. L. Chen, M. J. Park, P. Fragouli, H. Iatrou, N. Hadjichristidis, D. Cookson and N. P. Balsara, *Macromolecules*, 2007, **40**, 4578-4585.
65. M. J. Park and N. P. Balsara, *Macromolecules*, 2010, **43**, 292-298.
66. N. S. Wanakule, A. Panday, S. A. Mullin, E. Gann, A. Hexemer and N. P. Balsara, *Macromolecules*, 2009, **42**, 5642-5651.
67. A. Panday, S. Mullin, E. D. Gomez, N. Wanakule, V. L. Chen, A. Hexemer, J. Pople and N. P. Balsara, *Macromolecules*, 2009, **42**, 4632-4637.
68. F. S. Bates, *Science*, 1991, **251**, 898-905.
69. F. S. Bates and G. H. Fredrickson, *Annu. Rev. Phy. Chem.*, 1990, **41**, 525-557.
70. I. W. Hamley, *The Physics of Block Copolymers*, Oxford University Press, Oxford, 1998.
71. M. Muthukumar, C. K. Ober and E. L. Thomas, *Science*, 1997, **277**, 1225-1232.
72. O. Ikkala and G. T. Brinke, *Science*, 2002, **295**, 2407-2409.
73. S. Forster and T. Plantenberg, *Angew. Chem. Int. Ed.*, 2002, **41**, 688-714.
74. C. Park, J. Yoon and T. E. L., *Polymer*, 2003, 6725-6760.
75. I. W. Hamley, *Angew. Chem. Int. Ed.*, 2003, **42**, 1692-1712.
76. T. Liu, C. Burger and B. Chu, *Prog. Polym. Sci*, 2003, **28**, 5-26.
77. Y. Gu, S. Zhang, L. Martinetti, K. H. Lee, L. D. McIntosh, C. D. Frisbie and T. P. Lodge, *J. Am. Chem. Soc.*, 2013, **135**, 9652-9655.
78. J. Sax and J. M. Ottino, *Polym. Eng. Sci.*, 1983, **23**, 165-176.

79. P. W. Majewski, M. Gopinadhan and C. O. Osuji, *Soft Matter*, 2013, **9**, 7106-7116.
80. L. Ramon-Gimenez, R. Storz, J. Haberl, H. Finkelmann and A. Hoffmann, *Macromol. Rapid Commun.*, 2012, **33**, 386-391.
81. B.-K. Choi and Y.-W. Kim, *Electrochim. Acta*, 2004, **49**, 2307-2313.
82. M. Marzantowicz, J. R. Dygas, F. Krok, A. Łasińska, Z. Florjańczyk and E. Zygadło-Monikowska, *Electrochim. Acta*, 2006, **51**, 1713-1727.
83. Y. Zhang, J. Li, H. Huo and S. Jiang, *J. Appl. Polym. Sci.*, 2012, **123**, 1935-1943.
84. S. K. Fullerton-Shirey and J. K. Maranas, *Macromolecules*, 2009, **42**, 2142-2156.
85. S. Cheng, D. M. Smith and C. Y. Li, *Macromolecules*, 2014, **47**, 3978-3986.
86. D. Blundell, A. Keller and A. Kovacs, *J. Polym. Sci. B: Polym. Lett.*, 1966, **4**, 481-486.
87. P. Geil, *Polymer single crystal*, Interscience New York, 1963.
88. B. Li and C. Y. Li, *J. Am. Chem. Soc.*, 2007, **129**, 12-13.
89. C. Y. Li, *J. Poly. Sci. Poly. Phys.*, 2009, **47**, 2436-2440.
90. B. B. Wang, B. Li, R. C. M. Ferrier and C. Y. Li, *Macromol. Rapid Commun.*, 2010, **31**, 169-175.
91. B. B. Wang, B. Li, B. Dong, B. Zhao and C. Y. Li, *Macromolecules*, 2010, **43**, 9234-9238.
92. B. Li, B. B. Wang, R. C. M. Ferrier and C. Y. Li, *Macromolecules*, 2009, **42**, 9394-9399.
93. T. Zhou, B. Dong, H. Qi, S. Mei and C. Y. Li, *J. Polym. Sci. Poly. Phys.*, 2014, **52**, 1620-1640.
94. W. Wang and C. Y. Li, *ACS Macro. Lett.*, 2014, **3**, 175-179.
95. H. Qi, W. Wang and C. Y. Li, *ACS Macro. Lett.*, 2014, **3**, 675-678.
96. B. Dong, T. Zhou, H. Zhang and C. Y. Li, *ACS Nano*, 2013, **7**, 5192-5198.
97. B. Dong, W. Wang, D. L. Miller and C. Y. Li, *Journal of Materials Chemistry*, 2012, **22**, 15526-15529.
98. B. Dong, B. Li and C. Y. Li, *J. Mater. Chem.*, 2011, **21**, 13155-13158.
99. T. Zhou, B. Han, H. Qi, Q. Pan, D. M. Smith, L. Han and C. Y. Li, *Nanoscale*, 2018, **10**, 18269-18274.
100. S. Mei and C. Y. Li, *Angew. Chem. Int. Ed.*, 2018, DOI: doi:10.1002/anie.201809915, In Press.
101. S. Mei, H. Qi, T. Zhou and C. Y. Li, *Angew. Chem. Inter. Ed.* , 2017, **56**, 13645-13649.
102. B. Dong, D. L. Miller and C. Y. Li, *The Journal of Physical Chemistry Letters*, 2012, **3**, 1346-1350.
103. H. Qi, H. Zhou, Q. Tang, J. Y. Lee, Z. Fan, S. Kim, M. C. Staub, T. Zhou, S. Mei, L. Han, D. J. Pochan, H. Cheng, W. Hu and C. Y. Li, *Nature Communications*, 2018, **9**, 3005.
104. T. Zhou, H. Qi, L. Han, D. Barbash and C. Y. Li, *Nature Communications*, 2016, **7**, 11119.
105. W. Wang, H. Qi, T. Zhou, S. Mei, L. Han, T. Higuchi, H. Jinnai and C. Y. Li, *Nature Communications*, 2016, **7**, 10599-10599.
106. H. Qi, T. Zhou, S. Mei, X. Chen and C. Y. Li, *ACS Macro. Lett.*, 2016, **5**, 651-655.
107. L. E. Nielsen, *Journal of Macromolecular Science: Part A - Chemistry*, 1967, **1**, 929-942.
108. R. K. Bharadwaj, *Macromolecules*, 2001, **34**, 9189-9192.
109. B. Xu, Q. Zheng, Y. Song and Y. Shangguan, *Polymer*, 2006, **47**, 2904-2910.
110. M. Watanabe, S. Nagano, K. Sanui and N. Ogata, *Polym. J.*, 1986, **18**, 809-817.
111. L. R. Middleton, E. B. Trigg, L. Yan and K. I. Winey, *Polymer*, 2018, **144**, 184-191.
112. E. B. Trigg, T. W. Gaines, M. Maréchal, D. E. Moed, P. Rannou, K. B. Wagener, M. J. Stevens and K. I. Winey, *Nature Materials*, 2018, **17**, 725.
113. W. Krawiec, L. G. Scanlon Jr, J. P. Fellner, R. A. Vaia, S. Vasudevan and E. P. Giannelis, *J. Power Sources*, 1995, **54**, 310-315.
114. E. Quartarone, P. Mustarelli and A. Magistris, *Solid State Ionics*, 1998, **110**, 1-14.
115. W. Wieczorek, P. Lipka, G. Żukowska and H. Wyciślik, *J. Phys. Chem. B*, 1998, **102**, 6968-6974.
116. C. Capiglia, P. Mustarelli, E. Quartarone, C. Tomasi and A. Magistris, *Solid State Ionics*, 1999, **118**, 73-79.
117. B. Kumar and L. G. Scanlon, *Solid State Ionics*, 1999, **124**, 239-254.
118. F. Croce, L. Persi, F. Ronci and B. Scrosati, *Solid State Ionics*, 2000, **135**, 47-52.

119. M. Marcinek, A. Bac, P. Lipka, A. Zalewska, G. Żukowska, R. Borkowska and W. Wieczorek, *J. Phys. Chem. B*, 2000, **104**, 11088-11093.
120. B. Scrosati, F. Croce and L. Persi, *J. Electrochem. Soc.*, 2000, **147**, 1718-1721.
121. S. Chung, Y. Wang, L. Persi, F. Croce, S. Greenbaum, B. Scrosati and E. Plichta, *J. Power Sources*, 2001, **97**, 644-648.
122. P. A. R. D. Jayathilaka, M. A. K. L. Dissanayake, I. Albinsson and B. E. Mellander, *Electrochim. Acta*, 2002, **47**, 3257-3268.
123. W. Wieczorek, Z. Florjanczyk and J. R. Stevens, *Electrochim. Acta*, 1995, **40**, 2251-2258.
124. M. Siekierski, W. Wieczorek and J. Przyłuski, *Electrochim. Acta*, 1998, **43**, 1339-1342.
125. Y. W. Kim, W. Lee and B. K. Choi, *Electrochim. Acta*, 2000, **45**, 1473-1477.
126. B.-K. Choi, Y.-W. Kim and K.-H. Shin, *J. Power Sources*, 1997, **68**, 357-360.
127. A. S. Best, A. Ferry, D. R. MacFarlane and M. Forsyth, *Solid State Ionics*, 1999, **126**, 269-276.
128. H. J. Walls, J. Zhou, J. A. Yerian, P. S. Fedkiw, S. A. Khan, M. K. Stowe and G. L. Baker, *J. Power Sources*, 2000, **89**, 156-162.
129. A. S. Best, J. Adebahr, P. Jacobsson, D. R. MacFarlane and M. Forsyth, *Macromolecules*, 2001, **34**, 4549-4555.
130. P. Johansson, M. A. Ratner and D. F. Shriver, *J. Phys. Chem. B*, 2001, **105**, 9016-9021.
131. J. Xie, R. G. Duan, Y. Han and J. B. Kerr, *Solid State Ionics*, 2004, **175**, 755-758.
132. M. Moniruzzaman and K. I. Winey, *Macromolecules*, 2006, **39**, 5194-5205.
133. E. D. Laird and C. Y. Li, *Macromolecules* 2013, **46**, 2877-2891.
134. Z. Huang, S. Wang, S. Kota, Q. Pan, M. W. Barsoum and C. Y. Li, *Polymer*, 2016, **102**, 119-126.
135. Q. Pan, Y. Zheng, S. Kota, W. Huang, S. Wang, H. Qi, S. Kim, Y. Tu, M. W. Barsoum and C. Y. Li, *Nanoscale Advances*, 2019, **1**, 395-402.
136. E. Ruizhitzky and P. Aranda, *Adv. Mater.*, 1990, **2**, 545-547.
137. P. Aranda, J. C. Galvan, B. Casal and E. Ruizhitzky, *Electrochim. Acta*, 1992, **37**, 1573-1577.
138. J. C. Hutchison, R. Bissessur and D. F. Shriver, *Chem. Mater.*, 1996, **8**, 1597-&.
139. J. L. Lutkenhaus, E. A. Olivetti, E. A. Verploegen, B. M. Cord, D. R. Sadoway and P. T. Hammond, *Langmuir*, 2007, **23**, 8515-8521.
140. M. Yuan, J. Erdman, C. Tang and H. Ardebili, *RSC Advances*, 2014, **4**, 59637-59642.
141. S. Gao, J. Zhong, G. Xue and B. Wang, *J. Membr. Sci.*, 2014, **470**, 316-322.
142. Y.-C. Cao, C. Xu, X. Wu, X. Wang, L. Xing and K. Scott, *J. Power Sources*, 2011, **196**, 8377-8382.
143. J. Shim, D.-G. Kim, H. J. Kim, J. H. Lee, J.-H. Baik and J.-C. Lee, *J. Mater. Chem. A*, 2014, **2**, 13873-13883.
144. S. Cheng, D. M. Smith and C. Y. Li, *Macromolecules*, 2015, **48**, 4503-4510.

Table of contents

The significance of the morphological control on ion transport properties of semicrystalline solid polymer electrolytes is illustrated.

Xiaowei Li received his Ph. D. in Applied Chemistry from Shanghai Jiao Tong University, China. He is currently a postdoc researcher at Drexel University under the supervision of Prof. Christopher Li. His research interest is focused on polymer electrolytes for lithium batteries.

Shan Cheng completed her B.S. degree in Polymer Science and Engineering at Jilin University, Changchun, China in 2009. She recently received her Ph.D. degree in Materials Science and Engineering from Drexel University under the supervision of Dr. Christopher Li. Her research is focused on understanding the correlation between crystalline morphology and ion transport in semi-crystalline solid polymer electrolytes.

Yongwei Zheng received his BS degree in Polymer Science from Fudan University in 2012, China and MS degree in Materials Science from University of Pennsylvania in 2014. He worked as scientist in TE Connectivity from 2014 to 2016. Currently, he is completing a Ph.D in Materials Science at Drexel University under the direction of Dr. Christopher Li. His research is focused on developing solid polymer electrolyte for high-performance lithium ion battery,

Christopher Li is a Professor in the Department of Materials Science and Engineering at Drexel University. He received his B.S. degree in Polymer Chemistry from the University of Science and Technology of China in 1995 and his Ph.D. in Polymer Science from the University of Akron in 1999. His research interests center on the structure and morphology of polymers and soft materials. He is a Fellow of the American Physical Society the North American Thermal Analysis Society.